

IMDPROMPTER: ADAPTING SAM TO IMAGE MANIPULATION DETECTION BY CROSS-VIEW AUTOMATED PROMPT LEARNING

Quan Zhang^{1*}, Yuxin Qi^{2*}, Xi Tang¹, Jinwei Fang³, Xi Lin², Ke Zhang^{1†}, Chun Yuan^{1†}

¹Tsinghua University ²Shanghai Jiao Tong University

³University of Science and Technology of China

{zhangqua22, ke-zhang19}@mails.tsinghua.edu.cn,
qiyuxin98@sjtu.edu.cn, yuanc@sz.tsinghua.edu.cn

ABSTRACT

Using extensive training data from SA-1B, the Segment Anything Model (SAM) has demonstrated exceptional generalization and zero-shot capabilities, attracting widespread attention in areas such as medical image segmentation and remote sensing image segmentation. However, its performance in the field of image manipulation detection remains largely unexplored and unconfirmed. There are two main challenges in applying SAM to image manipulation detection: a) reliance on manual prompts, and b) the difficulty of single-view information in supporting cross-dataset generalization. To address these challenges, we develop a cross-view prompt learning paradigm called IMDPrompter based on SAM. Benefiting from the design of automated prompts, IMDPrompter no longer relies on manual guidance, enabling automated detection and localization. Additionally, we propose components such as Cross-view Feature Perception, Optimal Prompt Selection, and Cross-View Prompt Consistency, which facilitate cross-view perceptual learning and guide SAM to generate accurate masks. Extensive experimental results from five datasets (CASIA, Columbia, Coverage, IMD2020, and NIST16) validate the effectiveness of our proposed method.

1 INTRODUCTION

With the continuous emergence of powerful editing tools, image manipulation has become unprecedentedly simple. These new opportunities have sparked the creativity of both benevolent and malicious users. In the past, organizing multimedia misinformation activities required complex skills, with attackers limited to splicing, copying, or deleting objects. Today, the rapid development of deep learning has made image editing tools more user-friendly and powerful, enabling users to quickly generate images of fictitious characters or create convincing deepfakes. Generative models can produce realistic image edits based on natural language prompts, perfectly matching inserted elements with the style and lighting of the environment Avrahami et al. (2023); Nichol et al. (2021).

However, the risks of these tools falling into the wrong hands are evident. In recent years, governments and funding agencies have shown increasing interest in developing forensic tools capable of addressing such attacks, particularly focusing on local image tampering that alters the semantic content of images Le et al. (2021). In response to these challenges, the fields of multimedia forensics and related sciences have rapidly expanded, proposing various methods and tools for image manipulation detection (IMD) and localization Guillaro et al. (2023). Despite significant progress in this area, the performance of state-of-the-art detectors in practical applications remains insufficient, primarily limited by several shortcomings that require further research: a) limited generalization ability; b) limited robustness; c) poor detection performance.

To address the shortcomings of existing IMD methods, we turn our attention to foundational models Kirillov et al. (2023); Radford et al. (2021); Jia et al. (2021); Sharif Razavian et al. (2014). Thanks to

*These authors contributed equally.

†Corresponding authors.

large-scale pretraining, foundational models like GPT-4 Achiam et al. (2023), Flamingo Alayrac et al. (2022), and SAM Kirillov et al. (2023) have made significant strides and contributed importantly to societal advancements. Among them, SAM, trained on one billion masks, demonstrates exceptional generalization ability, inspiring our research. However, using SAM for image manipulation detection tasks presents significant challenges: a) reliance on manual prompts: SAM’s interactive framework requires predefined prompts for input images, such as points, boxes, or masks. As a category-agnostic segmentation method, these limitations hinder SAM’s ability to achieve fully automated understanding in IMD tasks; b) single-view information struggles to support cross-dataset generalization: previous studies Zhou et al. (2020) have reported that DeepLabv2 Chen et al. (2017) trained on the CASIAv2 Dong et al. (2013) dataset performed well on the CAISAv1 Dong et al. (2013) dataset (sourced from CASIAv2) but poorly on the non-sourced COVER Wen et al. (2016) dataset. Similar behavior has also been observed with FCN Long et al. (2015) in this research.

To activate SAM’s IMD capabilities, we propose a cross-view automated prompt learning paradigm called IMDPrompter, aimed at learning how to generate prompts to enhance SAM’s functionality: a) Inspired by Battle & Gollapudi (2024) using automated prompt optimizers to improve the performance of LLMs, we constructed the automated prompt learning paradigm IMDPrompter, which generates prompt information automatically; b) To enhance SAM’s cross-dataset generalization ability, we introduced three noise views: SRM filtering, Bayer Conv, and Noiseprint, aiming to generate enhanced prompt information from multiple perspectives. To integrate information from multiple views, previous methods Zhai et al. (2023) employed a strategy of weighted averaging of the outputs from multiple views. However, due to the inaccuracy of prompts generated from individual views, simple weighted averaging can smooth out the accurate prompts from the optimal view to suboptimal ones. To preserve the accurate prompts from the optimal view, we propose an Optimal Prompt Selection (OPS) module based on minimizing localization loss; meanwhile, we noted that ideally, the prompt information from each view should converge toward the optimal prompt. Based on this motivation, we constructed a Cross-View Prompt Consistency (CPC) constraint to achieve alignment enhancement across views. For the mask generation process, we developed an Attention-based Cross-view Feature Perception (CFP) module and a Multi-Layer Perceptron-based Prompt Mixing module (PMM) to achieve the fusion of cross-view information and the integration of multiple types of prompts sequentially.

In summary, our main contributions are as follows.

- We are the first to apply SAM to the field of image manipulation detection and propose an automated prompt learning paradigm, IMDPrompter, eliminating the original SAM’s reliance on manual prompts.
- We propose modules such as Optimal Prompt Selection and Cross-View Prompt Consistency Constraint, achieving alignment enhancement across views.
- We propose Cross-view Feature Perception and Prompt Mixing modules, achieving the fusion of cross-view information and the integration of multiple types of prompts.

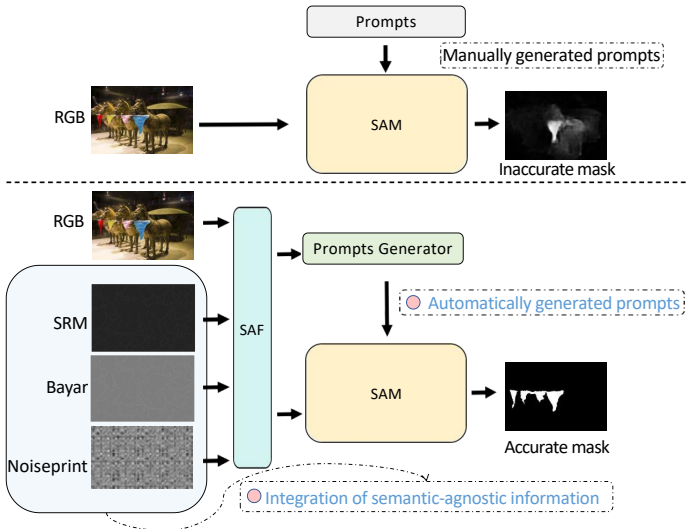


Figure 1: Improvements of proposed IMDPrompter over existing pipelines of baselines: (a). Automated prompt learning without the need for manual input. (b). Flexible integration of semantic-agnostic information crucial for Image Manipulation Detection.

- We demonstrate extensive results across five different image manipulation detection datasets, thoroughly validating the strong in-distribution and out-of-distribution image manipulation detection and localization capabilities of IMDPrompter.

2 RELATED WORK

Image Manipulation Detection. Currently, methods for image manipulation detection can be broadly categorized into two types, primarily distinguished by their recognition of manipulated artifacts. Some techniques Wu et al. (2019); Chen et al. (2021); Wu et al. (2022); Bi et al. (2019); Hu et al. (2020); Yang et al. (2020); Marra et al. (2020) rely on detecting abnormal features and often use high-pass noise filters Yang et al. (2020); Li & Huang (2019) to suppress content information. Other methods Park et al. (2018); Kwon et al. (2022); Mareen et al. (2022) attempt to detect inconsistencies in compression within tampered images, as they assume different compression Quality Factors (QFs) before and after the operation. Additionally, some researchers focus their attention on camera-based artifacts, such as model fingerprints Mareen et al. (2022); Cozzolino & Verdoliva (2019); Cozzolino et al. (2015).

Foundational Models. In recent years, foundational models have sparked a tremendous transformation in the field of artificial intelligence. These models, trained on extensive datasets, have demonstrated impressive zero-shot generalization capabilities across various scenarios Kirillov et al. (2023); Radford et al. (2021); Jia et al. (2021); Sharif Razavian et al. (2014). Renowned models such as Chat-GPT Ouyang et al. (2022), GPT-4 Achiam et al. (2023), and Stable Diffusion Rombach et al. (2022) have further propelled the development of artificial intelligence, making significant contributions to human civilization and exerting considerable influence across various industries. Inspired by the success of foundational models in natural language processing (NLP), researchers have begun exploring their potential applications in computer vision. While most of these models are aimed at extracting accessible knowledge from freely available data Alayrac et al. (2022); Radford et al. (2021); Chen et al. (2023), the recent SAM model Kirillov et al. (2023) adopts an innovative approach by constructing a data engine where the model co-develops annotations with environmental datasets. SAM uniquely leverages a vast collection of masks, showcasing robust generalization capabilities. However, it was initially designed as a task-agnostic segmentation model, requiring prompts (i.e., inputs of prior points, bounding boxes, or masks), and therefore does not directly facilitate end-to-end automated segmentation perception. This paper does not delve into the design and training of foundational image manipulation detection models; instead, we explore the potential of utilizing SAM’s powerful universal segmentation capabilities for image manipulation detection and localization. Furthermore, the proposed method of learning prompts can be extended to other visual foundational models beyond SAM.

Prompt Learning. In the past, machine learning tasks were primarily focused on fully supervised learning, where task-specific models were trained only on labeled instances of the target task Krizhevsky et al. (2017). However, over time, there has been a significant shift in learning paradigms, transitioning from fully supervised learning towards *pretraining and fine-tuning* approaches for downstream tasks. This shift allows models to leverage general features acquired during pretraining Russakovsky et al. (2015); Simonyan & Zisserman (2014); He et al. (2016). More recently, with the advent of foundational models, a new paradigm has emerged known as *pretraining and prompting* Chen et al. (2023); Lester et al. (2021); Liu et al. (2023); Zhou et al. (2022). In this paradigm, researchers no longer train models specifically for downstream tasks but instead redesign inputs using prompts to reformulate the downstream tasks to align with the original pretraining task Radford et al. (2021); Devlin et al. (2018); Radford et al. (2019). Prompting helps to reduce semantic gaps, bridge the gap between pretraining and fine-tuning, and prevent overfitting of the heads. Since the advent of GPT-3 Brown et al. (2020), prompting has evolved from traditional discrete Liu et al. (2023) and continuous prompt constructions Chen et al. (2023); Zhou et al. (2022) to large-scale model-centric contextual learning Alayrac et al. (2022), instruction tuning Liu et al. (2024); Peng et al. (2023); Gupta et al. (2022), and chaining approaches Wei et al. (2022); Wang et al. (2022a); Zhang et al. (2022). Currently, methods for constructing prompts include manual templates, heuristic-based templates, generation, fine-tuning word embeddings, and pseudo-labeling Liu et al. (2023); Wang et al. (2022b). In this paper, we propose a prompt generator for generating prompts compatible with SAM.

3 PROPOSED METHOD

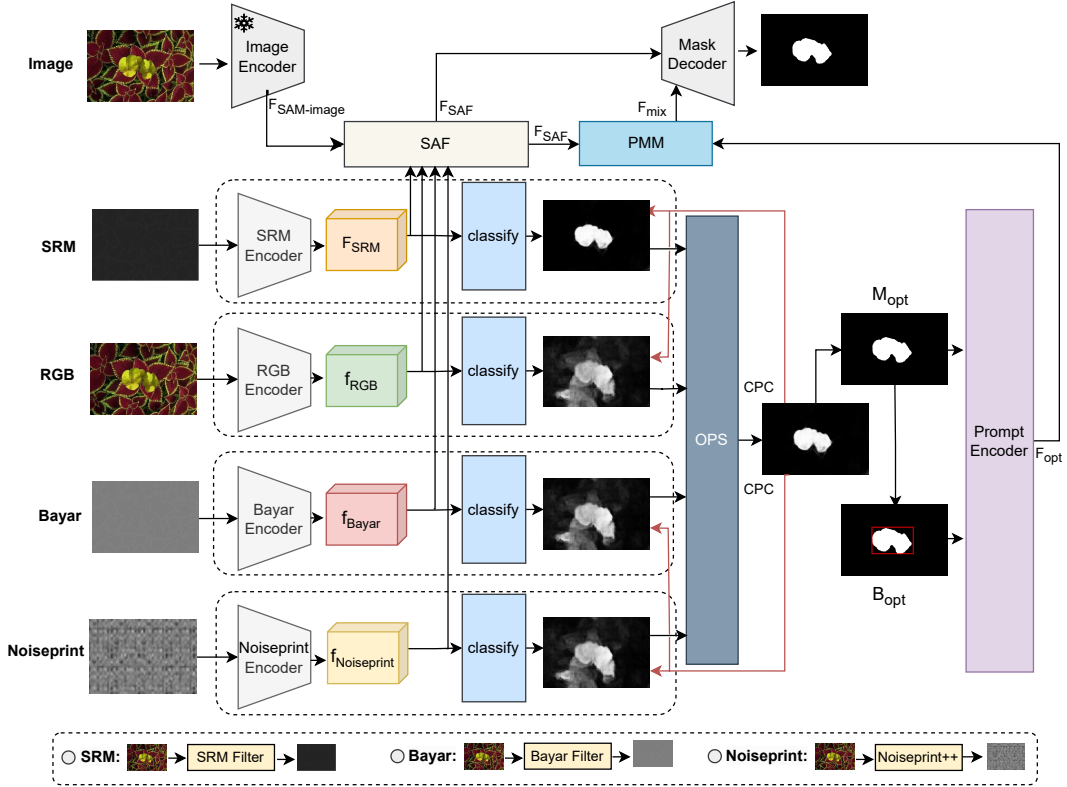


Figure 2: Overall framework of IMDPrompter. The prompter part consists of four views: RGB, SRM, Bayer and Noiseprint. OPS selects the optimal prediction from the four views to generate the best prompt. CPC enhances cross-view consistency. CFP achieves cross-view feature perception fusion. PMM achieves a mixture of multiple prompt information.

As shown in Figure 2, we established the automated prompt learning paradigm IMDPrompter based on cross-view perception learning, activating the automated detection and localization capabilities of SAM. Specifically, through the optimal prompt selection module, we heuristically select the best prompts from multiple prompts. By employing cross-view prompt consistency, we achieve enhanced alignment across views. Through the cross-view feature perception module and the prompt mixing module, we successively implement cross-view feature perception fusion and the mixing of various prompt information, thereby enabling efficient automated image manipulation detection and localization based on SAM.

3.1 MULTI-VIEW FEATURE REPRESENTATION

Current technology Zhou et al. (2020) finds that exploring semantic information from RGB views works well for in-domain (IND) manipulation detection but performs poorly in out-of-domain (OOD) detection. Additionally, utilizing noise views to learn semantic-agnostic information can yield strong performance. Given these findings, we believe that relying solely on RGB view information is insufficient for detecting and localizing manipulations. To address this issue, we introduce information from three semantic-agnostic views: the SRM noise view, the Bayer noise view, and the Noiseprint noise view, with the process as follows:

$$F_{\text{sam}} = \Phi_{\text{sam-img}}(\mathcal{I}) \quad (1)$$

$$f_{\text{RGB}} = \Phi_{\text{Seg-RGB}}(\mathcal{I}), f_{\text{SRM}} = \Phi_{\text{Seg-SRM}}(\Phi_{\text{SRM}}(\mathcal{I})), f_{\text{Bayer}} = \Phi_{\text{Seg-Bayer}}(\Phi_{\text{Bayer}}(\mathcal{I})) \quad (2)$$

$$f_{\text{Noiseprint}} = \Phi_{\text{Seg-Noiseprint}}(\Phi_{\text{Noiseprint}}(\mathcal{I})) \quad (3)$$

In the system, \mathcal{I} represents the input image, and $\Phi_{\text{sam-img}}$ denotes the SAM image encoder. F_{sam} represents the features encoded by the SAM image encoder. Φ_{SRM} , Φ_{Bayer} and $\Phi_{\text{Noiseprint}}$ respectively represent the SRM noise map extractor, the Bayer noise map extractor and the Noiseprint noise map extractor. $\Phi_{\text{Seg-RGB}}$, $\Phi_{\text{Seg-SRM}}$, $\Phi_{\text{Seg-Bayer}}$ and $\Phi_{\text{Seg-Noiseprint}}$ each represent the segmenter for the RGB view, SRM view, Bayer view and Noiseprint view, with all four segmenters having identical structures but non-shared parameters. f_{RGB} , f_{SRM} , f_{Bayer} and $f_{\text{Noiseprint}}$ represent the features from the RGB, SRM, Bayer, and Noiseprint views, respectively.

3.2 OPTIMAL PROMPT SELECTION

In the process of generating masked prompts, we utilize the mask probability distributions from four views, P_{RGB} , P_{SRM} , P_{Bayer} , and $P_{\text{Noiseprint}}$, and construct an integrated mask probability distribution P_{Ens} . We then select the optimal mask probability segmentation P_{opt} based on the principle of minimizing segmentation loss. Further, we obtain the mask M_{opt} and bounding box prompts \mathcal{B}_{opt} , which are input into SAM’s prompt encoder to obtain the prompt encoding F_{opt} . The process is as follows:

$$P_{\text{RGB}} = \Phi_{\text{RGB-CLS}}(f_{\text{RGB}}), P_{\text{SRM}} = \Phi_{\text{SRM-CLS}}(f_{\text{SRM}}), P_{\text{SRM}} = \Phi_{\text{SRM-CLS}}(f_{\text{SRM}}) \quad (4)$$

$$P_{\text{Noiseprint}} = \Phi_{\text{Noiseprint-CLS}}(f_{\text{Noiseprint}}), \quad (5)$$

$$P_{\text{Ens}} = \frac{P_{\text{RGB}} + P_{\text{SRM}} + P_{\text{Bayer}} + P_{\text{Noiseprint}}}{4}, \quad (6)$$

$$P_{\text{opt}} = \underset{P \in \mathcal{P}}{\text{argmin}} \mathcal{L}_{\text{Seg}}(P, G), \mathcal{P} = \{P_{\text{RGB}}, P_{\text{SRM}}, P_{\text{Bayer}}, P_{\text{Noiseprint}}, P_{\text{Ens}}\}, \quad (7)$$

$$M_{\text{opt}} = \Phi_{\text{mask}}(P_{\text{opt}}), \mathcal{B}_{\text{opt}} = \Phi_{\text{box}}(M_{\text{opt}}) \quad (8)$$

$$F_{\text{opt}} = \Phi_{\text{p-enc}}(M_{\text{opt}}, \mathcal{B}_{\text{opt}}), \quad (9)$$

where $\Phi_{\text{RGB-CLS}}$, $\Phi_{\text{SRM-CLS}}$, $\Phi_{\text{Bayer-CLS}}$ and $\Phi_{\text{Noiseprint-CLS}}$ represent classifiers for the RGB, SRM, Bayer, and Noiseprint views, respectively, G represents the one-hot encoded mask labels, \mathcal{L}_{Seg} is the segmentation loss function, Φ_{mask} represents the mask generation operation, Φ_{box} is the bounding box generation operation, and $\Phi_{\text{p-enc}}$ represents SAM’s prompt encoder.

3.3 CROSS-VIEW PROMPT CONSISTENCY

Ideally, the segmentation masks from the four views should be consistent with the optimal segmentation mask. Therefore, we constructed a cross-view prompt consistency enhancement loss to achieve enhanced prompt consistency across views. The CPC loss function is expressed as follows:

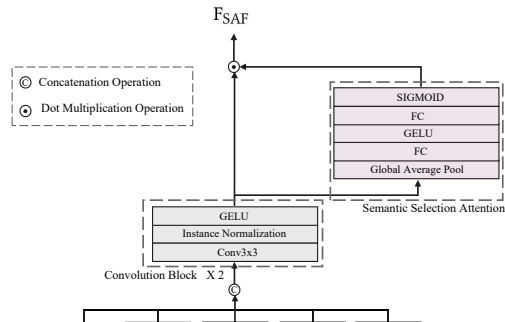
$$\mathcal{L}_{\text{CPC}} = \mathcal{L}_{\text{Seg}}(P_{\text{RGB}}, P_{\text{opt}}) + \mathcal{L}_{\text{Seg}}(P_{\text{SRM}}, P_{\text{opt}}) + \mathcal{L}_{\text{Seg}}(P_{\text{Bayer}}, P_{\text{opt}}) + \mathcal{L}_{\text{Seg}}(P_{\text{Noiseprint}}, P_{\text{opt}}), \quad (10)$$

where \mathcal{L}_{Seg} is the segmentation loss function.

3.4 CROSS-VIEW FEATURE PERCEPTION

Regarding the decoding process of SAM, relying solely on RGB view information is insufficient for generating accurate segmentation masks. Therefore, we propose a cross-view feature perception (CFP) module that integrates cross-view perception features from RGB, SRM, Bayer, and Noiseprint views, providing rich feature representations for the decoding process of SAM. The entire process is illustrated in Figure 3. Φ_{CFP} represents the cross-view feature perception module, while F_{CFP} denotes the features after cross-view perception fusion. The structure diagram of the CFP module is shown in Figure 3.

First, the features f_{RGB} , f_{SRM} , f_{Bayer} , and $f_{\text{Noiseprint}}$ are aligned with F_{sam} through bicubic interpolation, followed by channel concatenation with F_{sam} after passing through a 1×1 convolution. The concatenated features then pass through two stacked convolution blocks (comprising 3×3 convolution, instance normalization, and GELU activation),



and the output from the semantic selection attention branch (consisting of global average pooling, a fully connected layer, GELU, and sigmoid) is weighted onto the shortcut branch to produce the integrated feature F_{CFP} . Through the CFP module, features from multiple views are effectively integrated.

$$F_{\text{CFP}} = \Phi_{\text{CFP}}(F_{\text{sam}}, f_{\text{RGB}}, f_{\text{SRM}}, f_{\text{Bayer}}, f_{\text{Noiseprint}}) \quad (11)$$

3.5 PROMPT MIXING MODULE

Since F_{CFP} aggregates semantically related and unrelated features, it aids the guidance of SAM for image manipulation detection. Therefore, we constructed the PMM module, which is primarily based on MLP, to integrate multiple types of prompt information. First, the two types of prompt inputs, F_{CFP} and F_{opt} , are concatenated, followed by an MLP layer to perform dimension transformation to align with the original SAM prompt encoder’s prompt embedding. Then, F_{mix} and F_{CFP} are input into SAM’s mask decoder to achieve the image manipulation localization process. The process is as follows:

$$F_{\text{mix}} = \Phi_{\text{MLP}}([F_{\text{CFP}}; F_{\text{opt}}]), \quad (12)$$

$$P_{\text{sam}} = \Phi_{\text{sam-dec}}(F_{\text{CFP}}, F_{\text{mix}}), \quad (13)$$

where Φ_{MLP} represents the MLP layer operation, F_{mix} represents the integrated prompt embedding, and $\Phi_{\text{sam-dec}}$ represents SAM’s mask decoder, with P_{sam} representing the mask probability prediction output of the mask decoder.

3.6 TRAINING AND INFERENCE PIPELINE

The training loss function of IMDPrompter includes the segmentation loss from four prompt views $\mathcal{L}_{\text{Seg-p}}$, the CPC loss \mathcal{L}_{CPC} , the SAM decoder segmentation loss $\mathcal{L}_{\text{Seg-sam}}$, and the image-level prediction loss $\mathcal{L}_{\text{Img-level}}$. The formula is expressed as follows:

$$\mathcal{L} = \mathcal{L}_{\text{Seg-sam}} + \lambda_1 \mathcal{L}_{\text{Seg-p}} + \lambda_2 \mathcal{L}_{\text{CPC}} + \lambda_3 \mathcal{L}_{\text{Img-level}}, \quad (14)$$

where

$$L_{\text{Seg-sam}} = L_{\text{Seg}}(P_{\text{sam}}, G), \quad (15)$$

$$L_{\text{Seg-p}} = L_{\text{Seg}}(P_{\text{RGB}}, G) + L_{\text{Seg}}(P_{\text{Bayer}}, G) + L_{\text{Seg}}(P_{\text{SRM}}, G) + L_{\text{Seg}}(P_{\text{Noiseprint}}, G). \quad (16)$$

In this paper, we use Focal Loss as our L_{Seg} .

For image-level detection, following the work of Zhai et al. (2023), we adopt an adaptive pooling based on minimizing intra-class prediction variance. The overall computational process is as follows, first using Otsu’s method Otsu et al. (1975) to find a threshold ω_0 that minimizes the intra-class prediction variance:

$$\omega_0 = \arg \min_{\omega \in \{\hat{p}_{i,j}\}} |\{\hat{p}_{i,j} \mid \hat{p}_{i,j} < \omega\}| \text{var}(\{\hat{p}_{i,j} \mid \hat{p}_{i,j} < \omega\}) + |\{\hat{p}_{i,j} \mid \hat{p}_{i,j} \geq \omega\}| \text{var}(\{\hat{p}_{i,j} \mid \hat{p}_{i,j} \geq \omega\}), \quad (17)$$

where $\text{var}(\cdot)$ denotes variance, $\hat{p}_{i,j}$ is the pixel-level response at position (i, j) . Then the image-level prediction is aggregated from pixel-level responses above the threshold and the image-level loss is:

$$\hat{y}_A = \frac{1}{|\mathbb{P}_h|} \sum_{\hat{p} \in \mathbb{P}_h} \hat{p}; \mathbb{P}_h = \{\hat{p}_{i,j} \mid \hat{p}_{i,j} \geq \omega_0\}, \quad (18)$$

$$\mathcal{L}_{\text{Img-level}} = \mathcal{L}_{\text{BCE}}(y, \hat{y}_A), \quad (19)$$

where \hat{y}_A is the image-level prediction, \mathcal{L}_{BCE} denotes the binary cross-entropy loss.

During the inference process of IMDPrompter, since there are no true labels, our OPS module defaults to selecting P_{Ens} for generating masks and bounding box prompts, with other components functioning as during the training process.

4 EXPERIMENT

Dataset. Our method is trained only on the CASIAv2 dataset Dong et al. (2013). For in-distribution (IND) evaluation, we use the CASIAv1 dataset Dong et al. (2013). For out-of-distribution (OOD) evaluation, we use three datasets: Columbia Hsu & Chang (2006), Coverage Wen et al. (2016) and IMD2020 Novozamsky et al. (2020).

Evaluation Metrics. For image-level manipulation detection, we report specificity, sensitivity, and their F1-score (I-F1). The area under the receiver operating characteristic curve (AUC) is also reported as a threshold-independent metric for image-level detection. For pixel-level manipulation localization, we follow previous methods Chen et al. (2021); Zhou et al. (2018b;a); Salloum et al. (2018) to compute pixel accuracy, recall, and their F1-score (P-F1) on manipulated images. The overall performance of image and pixel-level manipulation detection/localization is measured by the harmonic mean of pixel-level and image-level F1-scores Chen et al. (2021), denoted as composite F1 (C-F1), and is sensitive to lower values of P-F1 and I-F1. To ensure fair comparison, a default threshold of 0.5 is used for F1 computation unless otherwise specified.

Implementation Details. In our experiments, unless otherwise specified, we consistently use the ViT backbone of SAM and employ FCN (lightweight architecture based on MobileNet Howard (2017)) as the segmentor for the three prompt views. We maintain image size at 1024×1024, consistent with the original input of the SAM model. To augment training samples, we use data augmentation techniques such as horizontal flipping and random cropping. The image encoder remains frozen during the training phase. All experiments are run on NVIDIA A6000 GPUs. For the optimization process, we train our model using the AdamW optimizer with an initial learning rate of 1e-4. We use a batch size of 4 and train for 100 epochs. We implement a linear warm-up strategy with a cosine annealing scheduler Loshchilov & Hutter (2016) to decay the learning rate.

4.1 COMPARISON WITH STATE-OF-THE-ART METHOD

Table 1: Pixel-level manipulation detection performance. Performance metric is F1-score (%). The best results for each test set are highlighted in bold and second-best values are underlined.

Method	Best threshold						Fixed threshold (0.5)					
	CASIA	COVER	Columbia	IMD	NIST	MEAN	CASIA	COVER	Columbia	IMD	NIST	MEAN
MFCN Salloum et al. (2018)	54.1	-	61.2	-	-	-	-	-	-	-	-	-
RGB-N Zhou et al. (2018b)	40.8	37.9	-	-	-	-	-	-	-	-	-	-
H-LSTM Bappy et al. (2019)	20.9	21.3	14.2	31.0	46.6	26.80	15.4	16.3	13.0	19.5	35.4	19.92
ManTra-Net Wu et al. (2019)	69.2	77.2	70.9	70.5	45.5	66.66	15.5	28.6	36.4	18.7	0.0	19.84
HP-FCN Li & Huang (2019)	21.4	19.9	47.1	16.9	36.0	28.26	15.4	0.3	6.7	11.2	12.1	9.14
CR-CNN Yang et al. (2020)	66.2	47.0	70.4	60.0	42.8	57.28	40.5	29.1	43.6	<u>26.2</u>	23.8	32.64
GSR-Net Zhou et al. (2018a)	57.4	48.9	62.2	68.7	45.6	56.56	38.7	28.5	61.3	24.3	28.3	36.22
SPAN Hu et al. (2020)	68.8	71.8	77.4	69.6	68.3	71.18	18.4	17.2	48.7	17.0	22.1	24.68
CAT-Net Kwon et al. (2021)	57.3	48.5	77.6	51.7	59.9	59.00	13.6	12.9	55.5	5.4	17.9	21.06
MVSS-Net Chen et al. (2021)	<u>75.3</u>	<u>82.4</u>	70.3	<u>75.7</u>	<u>73.7</u>	<u>75.48</u>	45.2	45.3	63.8	26.0	29.2	<u>41.90</u>
Trufor Guillaro et al. (2023)	83.5	74.1	<u>82.1</u>	-	68.8	-	<u>73.7</u>	<u>60.0</u>	<u>85.9</u>	-	<u>39.9</u>	-
FCN Long et al. (2015)	74.2	57.3	58.6	64.5	50.7	61.06	44.1	19.9	22.3	21.0	16.7	24.80
IMDPrompter	85.1	83.5	87.3	76.3	74.6	81.36	76.3	63.6	87.3	30.6	41.1	59.78
	+10.9	+26.2	+28.7	+11.8	+23.9	+20.3	+32.2	+43.7	+65.0	+9.6	+24.4	+34.98

Table 2: Image-level manipulation detection performance. Decision threshold: 0.5. NIST16 is excluded as it lacks genuine images. The best results for each test set are highlighted in bold and second-best values are underlined.

Method	CASIA				COVER				Columbia				IMD				MEAN	
	AUC	Sen.	Spe.	F1	AUC	Sen.	Spe.	F1	AUC	Sen.	Spe.	F1	AUC	Sen.	Spe.	F1	AUC	F1
H-LSTM Bappy et al. (2019)	0.498	99.7	0.0	0.0	0.500	100.0	0.0	0.0	0.506	100.0	1.1	2.2	0.501	100.0	0.0	0.0	0.5013	0.55
ManTra-Net Wu et al. (2019)	0.500	100.0	0.0	0.0	0.500	100.0	0.0	0.0	0.701	100.0	0.0	0.0	0.500	100.0	0.0	0.0	0.5503	0.00
CR-CNN Yang et al. (2020)	0.719	93.0	13.9	24.2	0.566	96.7	7.0	13.1	0.783	96.1	24.6	39.2	0.615	92.9	12.3	21.7	0.6708	24.55
GSR-Net Zhou et al. (2018a)	0.500	99.4	0.0	0.0	0.515	100.0	0.0	0.0	0.502	100.0	1.1	2.2	0.500	100.0	0.0	0.0	0.5043	0.55
SPAN Hu et al. (2020)	0.500	100.0	0.0	0.0	0.500	100.0	0.0	0.0	0.500	100.0	0.0	0.0	0.500	100.0	0.0	0.0	0.5000	0.00
CAF-Net Kwon et al. (2021)	0.647	23.9	92.1	38.0	0.557	28.0	80.0	<u>41.5</u>	0.971	87.2	96.2	<u>91.5</u>	0.586	27.5	81.6	<u>41.1</u>	0.6903	53.03
MVSS-Net Chen et al. (2021)	<u>0.937</u>	61.5	98.8	<u>75.8</u>	0.731	94.0	14.0	24.4	0.980	66.9	100.0	80.2	<u>0.656</u>	91.5	22.0	35.5	<u>0.8260</u>	<u>53.98</u>
Trufor Guillaro et al. (2023)	0.916	-	-	-	<u>0.770</u>	-	-	-	0.996	-	-	-	-	-	-	-	-	-
FCN Long et al. (2015)	0.770	72.8	64.3	68.3	0.541	90.0	10.0	18.0	0.762	95.0	32.2	48.1	0.502	84.6	15.5	26.2	0.6438	40.15
IMDPrompter	0.978	91.6	99.3	77.3	0.796	96.8	61.3	70.3	<u>0.983</u>	97.3	91.6	93.6	0.671	71.6	73.2	63.7	0.8570	76.23
	+0.208	+18.8	+35.0	+9.0	+0.255	+6.8	+51.3	+52.3	+0.221	+2.3	+59.4	+45.5	+0.169	-13.0	+57.7	+37.5	+0.2132	+36.08

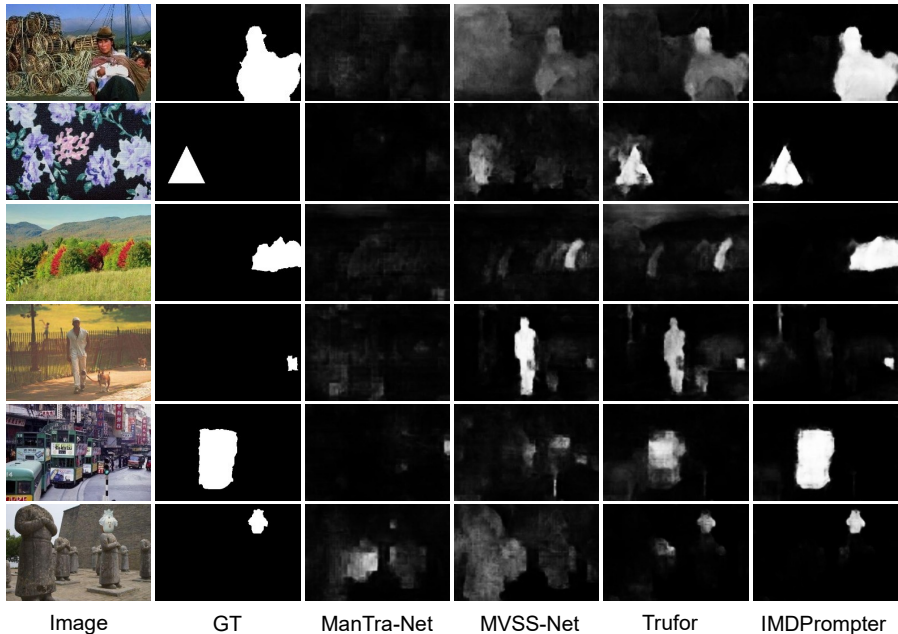


Figure 4: Visualization Comparison of Image Manipulation Detection and Localization Results

Table 3: Evaluation of each component of our method in IND dataset.

	CFP	CPC	OPS	PMM	CASIA		
					I-F1	P-F1	C-F1
1					70.6	70.3	70.4
2	✓				73.2	73.1	73.1
3	✓	✓			74.3	74.3	74.3
4	✓	✓	✓		75.1	76.1	75.6
5	✓	✓	✓	✓	77.3	76.3	76.8

Table 4: Evaluation of each component of our method in OOD dataset.

	CFP	CPC	OPS	PMM	COVER		
					I-F1	P-F1	C-F1
6					20.4	39.8	27.0
7	✓				49.6	54.3	51.8
8	✓	✓			58.6	57.0	57.8
9	✓	✓	✓		65.2	61.4	63.2
10	✓	✓	✓	✓	70.3	63.6	66.8

Pixel-level Manipulation Detection Table 1 illustrates the pixel-level detection performance of different models. We evaluate the F1-score under two settings: best threshold and fixed threshold (0.5). From Table 1, it is evident that IMDPrompter achieves the best performance across nearly all datasets. Under the optimal threshold setting, we achieved an average F1 Score of 81.36%. Under the fixed threshold setting, IMDPrompter achieved an average F1 Score of 59.78%, indicating that our proposed IMDPrompter demonstrates better robustness in threshold settings.

Image-level Manipulation Detection. Table 2 presents the image-level performance of different models. For image-level performance, we use a default decision threshold of 0.5. Once again, IMDPrompter emerges as the top performer, leveraging our prompt learning paradigm to achieve higher specificity in most test settings, thereby reducing false positives. Additionally, IMDPrompter achieves the best average AUC and average F1-scores. The average F1-score of IMDPrompter significantly surpasses that of the second-best method, MVSS-Net, with an improvement of 22.25%.

Qualitative Results. As shown in Figure 10, we visualized the image manipulation localization results of four methods: ManTra-Net, MVSS-Net, Trufor, and IMDPrompter. It is evident that IMDPrompter generates more accurate confidence maps for image manipulation localization, achieving better detection and localization.

4.2 ABLATION STUDIES

To reveal the impact of different components, we evaluated the proposed model under various settings, analyzing the distinct effects of each component on in-domain and out-of-domain datasets. As shown

Table 5: Ablation Study of View Combinations

RGB	Noiseprint	Bayer	SRM	CASIA				COVER				Columbia				IMD			
				I-AUC	I-F1	P-F1	C-F1	I-AUC	I-F1	P-F1	C-F1	I-AUC	I-F1	P-F1	C-F1	I-AUC	I-F1	P-F1	C-F1
✓				0.856	73.60	69.60	71.50	0.556	19.60	38.60	26.00	0.786	53.60	24.90	34.00	0.531	28.10	21.20	24.20
	✓			0.903	75.90	73.60	74.70	0.761	62.90	58.70	60.70	0.946	88.60	83.50	86.00	0.636	59.90	27.90	38.10
		✓		0.863	74.30	70.60	72.40	0.706	61.30	56.30	58.70	0.889	83.40	81.60	82.50	0.601	54.60	25.70	34.90
			✓	0.896	75.10	71.60	73.30	0.713	59.60	55.60	57.50	0.906	84.60	79.30	81.90	0.593	56.30	24.30	33.90
✓	✓			0.941	76.90	75.20	76.00	0.781	66.80	61.90	64.30	0.969	91.70	85.40	88.40	0.655	61.50	28.80	39.20
✓	✓	✓		0.962	77.10	75.90	76.50	0.788	68.70	62.40	65.40	0.977	92.40	86.50	89.40	0.660	62.60	29.50	40.10
✓	✓	✓	✓	0.978	77.30	76.30	76.80	0.796	70.30	63.60	66.80	0.983	93.60	87.30	90.30	0.671	63.70	30.60	41.30

Table 6: Ablation Study of SAM

Method	CASIA				COVER				Columbia				IMD			
	I-AUC	I-F1	P-F1	C-F1	I-AUC	I-F1	P-F1	C-F1	I-AUC	I-F1	P-F1	C-F1	I-AUC	I-F1	P-F1	C-F1
FCN	0.770	68.3	44.1	53.6	0.541	18.0	19.9	18.9	0.762	48.1	22.3	30.5	0.502	26.2	21.0	23.3
FCN+	0.873	73.4	61.3	66.8	0.681	49.2	43.9	46.4	0.871	72.6	52.4	60.9	0.589	43.1	25.1	31.7
IMDPrompter	0.978	77.3	76.3	76.8	0.796	70.3	63.6	66.8	0.983	93.6	87.3	90.3	0.671	63.7	30.6	41.3

in Tables 3 and 4, we conducted ablation experiments on the in-domain dataset CASIA and the out-of-domain dataset COVER, respectively.

Baseline. From *Experiment 1*, it is known that our baseline method achieved performance scores of 70.6%, 70.3%, and 70.4% on the I-F1, P-F1, and C-F1 metrics respectively in the CASIA dataset. In the COVER dataset, it scored 20.4%, 39.8%, and 27.0% on the same metrics. These experiments show that using only RGB visual view information has limited generalization ability in out-of-domain datasets.

Impact of CFP. From *Experiment 2*, By implementing cross-view feature perception fusion through the CFP module, the I-F1, P-F1, and C-F1 metrics on the CASIA dataset improved by 2.6%, 2.8%, and 2.7%, respectively. Experiment VII showed that on the COVER dataset, the I-F1, P-F1, and C-F1 metrics increased by 29.2%, 14.5%, and 24.8%, respectively. This indicates that cross-view feature perception fusion can enhance performance on both in-domain and out-of-domain datasets, especially on out-of-domain datasets.

Impact of CPC. From *Experiment 3*, the inclusion of CPC, which introduced cross-view consistency enhancement, resulted in performance gains of 3.7%, 4.0%, and 3.9% on the I-F1, P-F1, C-F1 metrics respectively in the CASIA dataset. Experiment VIII showed performance gains of 38.2%, 17.2%, and 30.8% respectively on the COVER dataset, confirming that the prompt information between different views is complementary and integrative enhancement can bring objective performance improvements.

Impact of OPS. The inclusion of OPS for heuristic selection of optimal prompts resulted in improvements of 4.5%, 5.8%, and 5.2% in the I-F1, P-F1, and C-F1 metrics on the CASIA dataset, respectively. Experiment IX showed gains of 44.8%, 21.6%, and 36.2% respectively on the COVER dataset, indicating that simply adding together prompts from different views is not enough to generate the best prompts, and a optimal prompts selection strategy can optimize the prompt selection process. From *Experiment 4*, the inclusion of OPS adaptive selection of the optimal prompts resulted in performance gains of 4.5%, 5.8%, and 5.2% on the I-F1, P-F1, C-F1 metrics respectively in the CASIA dataset.

Impact of PMM. From *Experiment 5*, with the inclusion of PMM which fully integrates various types of prompt information, there was an increase in performance of 6.7%, 6.0%, and 6.4% on the I-F1, P-F1, C-F1 metrics respectively in the CASIA dataset. *Experiment 10* showed an increase of 49.9%, 23.8%, and 39.8% respectively on the COVER dataset, further demonstrating the effectiveness of PMM.

Impact of View Combinations. As shown in Table 5, the performance of using the RGB view alone does not differ significantly from that of using semantic-agnostic views such as SRM, Bayer, and Noiseprint individually on the in-domain test set CASIA. In contrast, for the out-of-domain test sets COVER, Columbia, and IMD, there is a significant performance gap between the RGB view and the semantic-agnostic views. This indicates that semantic-agnostic views play a crucial role in generalization on out-of-domain datasets. Additionally, we conducted ablation studies on various view combinations, and using both the RGB view and the Noiseprint view simultaneously resulted in substantial performance improvements. This demonstrates that the Noiseprint view serves as a critical semantic-agnostic feature. Next, we sequentially introduced the Bayer and SRM views,

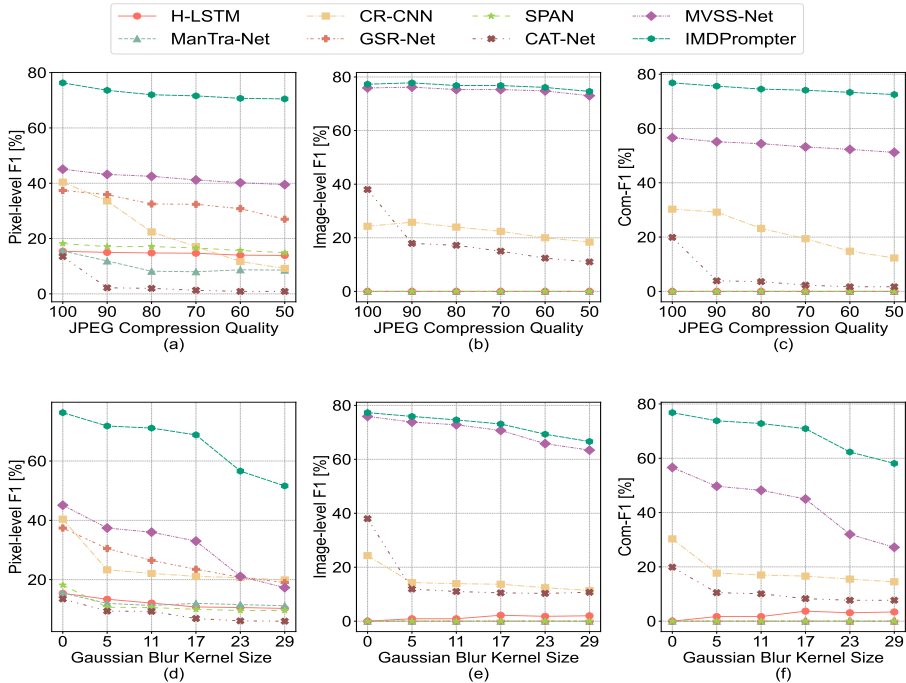


Figure 5: Robustness Analysis Against JPEG Compression and Gaussian Blur Interference

achieving further steady improvements across all metrics. When we combined the RGB, Noiseprint, SRM, and Bayer views, our method achieved optimal performance, validating the effectiveness of this combination.

Impact of SAM. As shown in Table 6, we constructed an FCN+ model that integrates four views without using SAM, further analyzing the impact of SAM on IMD. Due to the lack of potential priors from a large-scale pre-training dataset, the performance ceiling of FCN+ is relatively low. In contrast, our IMDPrompter fully leverages these potential priors, thereby enhancing the performance ceiling

Impact of Quality Degradation. As shown in Figure 5, following Dong et al. (2022), we evaluated the robustness of the models under two common image processing operations encountered during the dissemination of images on the internet, namely JPEG compression and Gaussian blur. Comparing these two operations, Gaussian blur has a more significant impact on detection performance, especially when using larger 17x17 scale convolution kernels. Compared to previous methods, our IMDPrompter exhibits better robustness.

5 CONCLUSION

In this paper, we propose a cross-view perceptual prompt learning paradigm, IMDPrompter, which applies SAM to the image manipulation detection task for the first time. We sequentially introduce components such as optimal prompt selection, cross-view prompt consistency, cross-view feature perception, and prompt mixing modules to achieve efficient and automated image manipulation detection and localization. Our IMDPrompter demonstrates significant image-level and pixel-level manipulation detection performance in both in-domain (IND) and out-of-domain (OOD) scenarios, as well as across various robustness evaluation settings.

REFERENCES

Josh Achiam, Steven Adler, Sandhini Agarwal, Lama Ahmad, Ilge Akkaya, Florencia Leoni Aleman, Diogo Almeida, Janko Altschmidt, Sam Altman, Shyamal Anadkat, et al. Gpt-4 technical report. *arXiv preprint arXiv:2303.08774*, 2023.

- Jean-Baptiste Alayrac, Jeff Donahue, Pauline Luc, Antoine Miech, Iain Barr, Yana Hasson, Karel Lenc, Arthur Mensch, Katherine Millican, Malcolm Reynolds, et al. Flamingo: a visual language model for few-shot learning. *Advances in neural information processing systems*, 35:23716–23736, 2022.
- Omri Avrahami, Ohad Fried, and Dani Lischinski. Blended latent diffusion. *ACM transactions on graphics (TOG)*, 42(4):1–11, 2023.
- Jawadul H Bappy, Cody Simons, Lakshmanan Nataraj, BS Manjunath, and Amit K Roy-Chowdhury. Hybrid lstm and encoder–decoder architecture for detection of image forgeries. *IEEE transactions on image processing*, 28(7):3286–3300, 2019.
- Rick Battle and Teja Gollapudi. The unreasonable effectiveness of eccentric automatic prompts. *arXiv preprint arXiv:2402.10949*, 2024.
- Xiuli Bi, Yang Wei, Bin Xiao, and Weisheng Li. Rru-net: The ringed residual u-net for image splicing forgery detection. In *Proceedings of the IEEE/CVF Conference on Computer Vision and Pattern Recognition Workshops*, pp. 0–0, 2019.
- Tom Brown, Benjamin Mann, Nick Ryder, Melanie Subbiah, Jared D Kaplan, Prafulla Dhariwal, Arvind Neelakantan, Pranav Shyam, Girish Sastry, Amanda Askell, et al. Language models are few-shot learners. *Advances in neural information processing systems*, 33:1877–1901, 2020.
- Keyan Chen, Xiaolong Jiang, Yao Hu, Xu Tang, Yan Gao, Jianqi Chen, and Weidi Xie. Ovarnet: Towards open-vocabulary object attribute recognition. In *Proceedings of the IEEE/CVF Conference on Computer Vision and Pattern Recognition*, pp. 23518–23527, 2023.
- Liang-Chieh Chen, George Papandreou, Iasonas Kokkinos, Kevin Murphy, and Alan L Yuille. Deeplab: Semantic image segmentation with deep convolutional nets, atrous convolution, and fully connected crfs. *IEEE transactions on pattern analysis and machine intelligence*, 40(4):834–848, 2017.
- Xinru Chen, Chengbo Dong, Jiaqi Ji, Juan Cao, and Xirong Li. Image manipulation detection by multi-view multi-scale supervision. In *Proceedings of the IEEE/CVF International Conference on Computer Vision*, pp. 14185–14193, 2021.
- Davide Cozzolino and Luisa Verdoliva. Noiseprint: A cnn-based camera model fingerprint. *IEEE Transactions on Information Forensics and Security*, 15:144–159, 2019.
- Davide Cozzolino, Giovanni Poggi, and Luisa Verdoliva. Splicebuster: A new blind image splicing detector. In *2015 IEEE International Workshop on Information Forensics and Security (WIFS)*, pp. 1–6. IEEE, 2015.
- Jacob Devlin, Ming-Wei Chang, Kenton Lee, and Kristina Toutanova. Bert: Pre-training of deep bidirectional transformers for language understanding. *arXiv preprint arXiv:1810.04805*, 2018.
- Chengbo Dong, Xinru Chen, Ruohan Hu, Juan Cao, and Xirong Li. Mvss-net: Multi-view multi-scale supervised networks for image manipulation detection. *IEEE Transactions on Pattern Analysis and Machine Intelligence*, 45(3):3539–3553, 2022.
- Jing Dong, Wei Wang, and Tieniu Tan. Casia image tampering detection evaluation database. In *2013 IEEE China summit and international conference on signal and information processing*, pp. 422–426. IEEE, 2013.
- Fabrizio Guillaro, Davide Cozzolino, Avneesh Sud, Nicholas Dufour, and Luisa Verdoliva. Trufor: Leveraging all-round clues for trustworthy image forgery detection and localization. In *Proceedings of the IEEE/CVF Conference on Computer Vision and Pattern Recognition*, pp. 20606–20615, 2023.
- Prakhar Gupta, Cathy Jiao, Yi-Ting Yeh, Shikib Mehri, Maxine Eskenazi, and Jeffrey P Bigham. Instructdial: Improving zero and few-shot generalization in dialogue through instruction tuning. *arXiv preprint arXiv:2205.12673*, 2022.

- Kaiming He, Xiangyu Zhang, Shaoqing Ren, and Jian Sun. Deep residual learning for image recognition. In *Proceedings of the IEEE conference on computer vision and pattern recognition*, pp. 770–778, 2016.
- Andrew G Howard. Mobilenets: Efficient convolutional neural networks for mobile vision applications. *arXiv preprint arXiv:1704.04861*, 2017.
- Yu-Feng Hsu and Shih-Fu Chang. Detecting image splicing using geometry invariants and camera characteristics consistency. In *2006 IEEE International Conference on Multimedia and Expo*, pp. 549–552. IEEE, 2006.
- Xuefeng Hu, Zhihan Zhang, Zhenye Jiang, Syomantak Chaudhuri, Zhenheng Yang, and Ram Nevatia. Span: Spatial pyramid attention network for image manipulation localization. In *Computer Vision—ECCV 2020: 16th European Conference, Glasgow, UK, August 23–28, 2020, Proceedings, Part XXI 16*, pp. 312–328. Springer, 2020.
- Chao Jia, Yinfei Yang, Ye Xia, Yi-Ting Chen, Zarana Parekh, Hieu Pham, Quoc Le, Yun-Hsuan Sung, Zhen Li, and Tom Duerig. Scaling up visual and vision-language representation learning with noisy text supervision. In *International conference on machine learning*, pp. 4904–4916. PMLR, 2021.
- Alexander Kirillov, Eric Mintun, Nikhila Ravi, Hanzi Mao, Chloe Rolland, Laura Gustafson, Tete Xiao, Spencer Whitehead, Alexander C Berg, Wan-Yen Lo, et al. Segment anything. In *Proceedings of the IEEE/CVF International Conference on Computer Vision*, pp. 4015–4026, 2023.
- Vladimir V Knyaz, Vladimir Knyaz, and Fabio Remondino. The point where reality meets fantasy: Mixed adversarial generators for image splice detection. *Advances in neural information processing systems*, 32, 2019.
- Alex Krizhevsky, Ilya Sutskever, and Geoffrey E Hinton. Imagenet classification with deep convolutional neural networks. *Communications of the ACM*, 60(6):84–90, 2017.
- Myung-Joon Kwon, In-Jae Yu, Seung-Hun Nam, and Heung-Kyu Lee. Cat-net: Compression artifact tracing network for detection and localization of image splicing. In *Proceedings of the IEEE/CVF Winter Conference on Applications of Computer Vision*, pp. 375–384, 2021.
- Myung-Joon Kwon, Seung-Hun Nam, In-Jae Yu, Heung-Kyu Lee, and Changick Kim. Learning jpeg compression artifacts for image manipulation detection and localization. *International Journal of Computer Vision*, 130(8):1875–1895, 2022.
- Trung-Nghia Le, Huy H Nguyen, Junichi Yamagishi, and Isao Echizen. Openforensics: Large-scale challenging dataset for multi-face forgery detection and segmentation in-the-wild. In *Proceedings of the IEEE/CVF international conference on computer vision*, pp. 10117–10127, 2021.
- Brian Lester, Rami Al-Rfou, and Noah Constant. The power of scale for parameter-efficient prompt tuning. *arXiv preprint arXiv:2104.08691*, 2021.
- Haodong Li and Jiwu Huang. Localization of deep inpainting using high-pass fully convolutional network. In *proceedings of the IEEE/CVF international conference on computer vision*, pp. 8301–8310, 2019.
- Haotian Liu, Chunyuan Li, Qingyang Wu, and Yong Jae Lee. Visual instruction tuning. *Advances in neural information processing systems*, 36, 2024.
- Pengfei Liu, Weizhe Yuan, Jinlan Fu, Zhengbao Jiang, Hiroaki Hayashi, and Graham Neubig. Pre-train, prompt, and predict: A systematic survey of prompting methods in natural language processing. *ACM Computing Surveys*, 55(9):1–35, 2023.
- Jonathan Long, Evan Shelhamer, and Trevor Darrell. Fully convolutional networks for semantic segmentation. In *Proceedings of the IEEE conference on computer vision and pattern recognition*, pp. 3431–3440, 2015.
- Ilya Loshchilov and Frank Hutter. Sgdr: Stochastic gradient descent with warm restarts. *arXiv preprint arXiv:1608.03983*, 2016.

- Jun Ma, Yuting He, Feifei Li, Lin Han, Chenyu You, and Bo Wang. Segment anything in medical images. *Nature Communications*, 15(1):654, 2024.
- Hannes Mareen, Dante Vanden Bussche, Fabrizio Guillaro, Davide Cozzolino, Glenn Van Wallendael, Peter Lambert, and Luisa Verdoliva. Comprint: Image forgery detection and localization using compression fingerprints. In *International Conference on Pattern Recognition*, pp. 281–299. Springer, 2022.
- Francesco Marra, Diego Gagnaniello, Luisa Verdoliva, and Giovanni Poggi. A full-image full-resolution end-to-end-trainable cnn framework for image forgery detection. *IEEE Access*, 8: 133488–133502, 2020.
- Alex Nichol, Prafulla Dhariwal, Aditya Ramesh, Pranav Shyam, Pamela Mishkin, Bob McGrew, Ilya Sutskever, and Mark Chen. Glide: Towards photorealistic image generation and editing with text-guided diffusion models. *arXiv preprint arXiv:2112.10741*, 2021.
- Adam Novozamsky, Babak Mahdian, and Stanislav Saic. Imd2020: A large-scale annotated dataset tailored for detecting manipulated images. In *Proceedings of the IEEE/CVF Winter Conference on Applications of Computer Vision Workshops*, pp. 71–80, 2020.
- Nobuyuki Otsu et al. A threshold selection method from gray-level histograms. *Automatica*, 11 (285-296):23–27, 1975.
- Long Ouyang, Jeffrey Wu, Xu Jiang, Diogo Almeida, Carroll Wainwright, Pamela Mishkin, Chong Zhang, Sandhini Agarwal, Katarina Slama, Alex Ray, et al. Training language models to follow instructions with human feedback. *Advances in neural information processing systems*, 35:27730–27744, 2022.
- Jinseok Park, Donghyeon Cho, Wonhyuk Ahn, and Heung-Kyu Lee. Double jpeg detection in mixed jpeg quality factors using deep convolutional neural network. In *Proceedings of the European conference on computer vision (ECCV)*, pp. 636–652, 2018.
- Baolin Peng, Chunyuan Li, Pengcheng He, Michel Galley, and Jianfeng Gao. Instruction tuning with gpt-4. *arXiv preprint arXiv:2304.03277*, 2023.
- Alec Radford, Jeffrey Wu, Rewon Child, David Luan, Dario Amodei, Ilya Sutskever, et al. Language models are unsupervised multitask learners. *OpenAI blog*, 1(8):9, 2019.
- Alec Radford, Jong Wook Kim, Chris Hallacy, Aditya Ramesh, Gabriel Goh, Sandhini Agarwal, Girish Sastry, Amanda Askell, Pamela Mishkin, Jack Clark, et al. Learning transferable visual models from natural language supervision. In *International conference on machine learning*, pp. 8748–8763. PMLR, 2021.
- Yuan Rao and Jiangqun Ni. Self-supervised domain adaptation for forgery localization of jpeg compressed images. In *Proceedings of the IEEE/CVF international conference on computer vision*, pp. 15034–15043, 2021.
- Nikhila Ravi, Valentin Gabeur, Yuan-Ting Hu, Ronghang Hu, Chaitanya Ryali, Tengyu Ma, Haitham Khedr, Roman Rädle, Chloe Rolland, Laura Gustafson, et al. Sam 2: Segment anything in images and videos. *arXiv preprint arXiv:2408.00714*, 2024.
- Robin Rombach, Andreas Blattmann, Dominik Lorenz, Patrick Esser, and Björn Ommer. High-resolution image synthesis with latent diffusion models. In *Proceedings of the IEEE/CVF conference on computer vision and pattern recognition*, pp. 10684–10695, 2022.
- Olga Russakovsky, Jia Deng, Hao Su, Jonathan Krause, Sanjeev Satheesh, Sean Ma, Zhiheng Huang, Andrej Karpathy, Aditya Khosla, Michael Bernstein, et al. Imagenet large scale visual recognition challenge. *International journal of computer vision*, 115:211–252, 2015.
- Ronald Salloum, Yuzhuo Ren, and C-C Jay Kuo. Image splicing localization using a multi-task fully convolutional network (mfcn). *Journal of Visual Communication and Image Representation*, 51: 201–209, 2018.

- Tal Shaharabany, Aviad Dahan, Raja Giryes, and Lior Wolf. Autosam: Adapting sam to medical images by overloading the prompt encoder. *arXiv preprint arXiv:2306.06370*, 2023.
- Ali Sharif Razavian, Hossein Azizpour, Josephine Sullivan, and Stefan Carlsson. Cnn features off-the-shelf: an astounding baseline for recognition. In *Proceedings of the IEEE conference on computer vision and pattern recognition workshops*, pp. 806–813, 2014.
- Karen Simonyan and Andrew Zisserman. Very deep convolutional networks for large-scale image recognition. *arXiv preprint arXiv:1409.1556*, 2014.
- Xuezhi Wang, Jason Wei, Dale Schuurmans, Quoc Le, Ed Chi, Sharan Narang, Aakanksha Chowdhery, and Denny Zhou. Self-consistency improves chain of thought reasoning in language models. *arXiv preprint arXiv:2203.11171*, 2022a.
- Zifeng Wang, Zizhao Zhang, Chen-Yu Lee, Han Zhang, Ruoxi Sun, Xiaoqi Ren, Guolong Su, Vincent Perot, Jennifer Dy, and Tomas Pfister. Learning to prompt for continual learning. In *Proceedings of the IEEE/CVF Conference on Computer Vision and Pattern Recognition*, pp. 139–149, 2022b.
- Jason Wei, Xuezhi Wang, Dale Schuurmans, Maarten Bosma, Fei Xia, Ed Chi, Quoc V Le, Denny Zhou, et al. Chain-of-thought prompting elicits reasoning in large language models. *Advances in neural information processing systems*, 35:24824–24837, 2022.
- Bihan Wen, Ye Zhu, Ramanathan Subramanian, Tian-Tsong Ng, Xuanjing Shen, and Stefan Winkler. Coverage—a novel database for copy-move forgery detection. In *2016 IEEE international conference on image processing (ICIP)*, pp. 161–165. IEEE, 2016.
- Haiwei Wu, Jiantao Zhou, Jinyu Tian, Jun Liu, and Yu Qiao. Robust image forgery detection against transmission over online social networks. *IEEE Transactions on Information Forensics and Security*, 17:443–456, 2022.
- Junde Wu, Wei Ji, Yuanpei Liu, Huazhu Fu, Min Xu, Yanwu Xu, and Yueming Jin. Medical sam adapter: Adapting segment anything model for medical image segmentation. *arXiv preprint arXiv:2304.12620*, 2023.
- Yue Wu, Wael AbdAlmageed, and Premkumar Natarajan. Mantra-net: Manipulation tracing network for detection and localization of image forgeries with anomalous features. In *Proceedings of the IEEE/CVF conference on computer vision and pattern recognition*, pp. 9543–9552, 2019.
- Enze Xie, Wenhai Wang, Zhiding Yu, Anima Anandkumar, Jose M Alvarez, and Ping Luo. Segformer: Simple and efficient design for semantic segmentation with transformers. *Advances in neural information processing systems*, 34:12077–12090, 2021.
- Chao Yang, Huizhou Li, Fangting Lin, Bin Jiang, and Hao Zhao. Constrained r-cnn: A general image manipulation detection model. In *2020 IEEE International conference on multimedia and expo (ICME)*, pp. 1–6. IEEE, 2020.
- Chao Yang, Zhiyu Wang, Huawei Shen, Huizhou Li, and Bin Jiang. Multi-modality image manipulation detection. In *2021 IEEE International conference on multimedia and expo (ICME)*, pp. 1–6. IEEE, 2021.
- Yuanhao Zhai, Tianyu Luan, David Doermann, and Junsong Yuan. Towards generic image manipulation detection with weakly-supervised self-consistency learning. In *Proceedings of the IEEE/CVF International Conference on Computer Vision*, pp. 22390–22400, 2023.
- Kaidong Zhang and Dong Liu. Customized segment anything model for medical image segmentation. *arXiv preprint arXiv:2304.13785*, 2023.
- Zhuosheng Zhang, Aston Zhang, Mu Li, and Alex Smola. Automatic chain of thought prompting in large language models. *arXiv preprint arXiv:2210.03493*, 2022.
- Hengshuang Zhao, Jianping Shi, Xiaojuan Qi, Xiaogang Wang, and Jiaya Jia. Pyramid scene parsing network. In *Proceedings of the IEEE conference on computer vision and pattern recognition*, pp. 2881–2890, 2017.

- Sixiao Zheng, Jiachen Lu, Hengshuang Zhao, Xiatian Zhu, Zekun Luo, Yabiao Wang, Yanwei Fu, Jianfeng Feng, Tao Xiang, Philip HS Torr, et al. Rethinking semantic segmentation from a sequence-to-sequence perspective with transformers. In *Proceedings of the IEEE/CVF conference on computer vision and pattern recognition*, pp. 6881–6890, 2021.
- Kaiyang Zhou, Jingkang Yang, Chen Change Loy, and Ziwei Liu. Learning to prompt for vision-language models. *International Journal of Computer Vision*, 130(9):2337–2348, 2022.
- Peng Zhou, B Chen, Xintong Han, Mahyar Najibi, and Larry S Davis. Generate, segment and replace: Towards generic manipulation segmentation. *arXiv preprint arXiv:1811.09729*, 2018a.
- Peng Zhou, Xintong Han, Vlad I Morariu, and Larry S Davis. Learning rich features for image manipulation detection. In *Proceedings of the IEEE conference on computer vision and pattern recognition*, pp. 1053–1061, 2018b.
- Peng Zhou, Bor-Chun Chen, Xintong Han, Mahyar Najibi, Abhinav Shrivastava, Ser-Nam Lim, and Larry Davis. Generate, segment, and refine: Towards generic manipulation segmentation. In *Proceedings of the AAAI conference on artificial intelligence*, volume 34, pp. 13058–13065, 2020.
- Xueyan Zou, Jianwei Yang, Hao Zhang, Feng Li, Linjie Li, Jianfeng Wang, Lijuan Wang, Jianfeng Gao, and Yong Jae Lee. Segment everything everywhere all at once. *Advances in Neural Information Processing Systems*, 36, 2024.

6 APPENDIX

6.1 LIMITATIONS AND BROADER IMPACTS

Limitations. We have some limitations in our method. First, it cannot detect completely generated images. Second, training IMDPrompter requires complete pixel-level supervision. In future research, we plan to explore more efficient label utilization through weakly supervised and semi-supervised learning approaches and extend these methods to newer foundational models such as SEEMZou et al. (2024) and SAM2 Ravi et al. (2024).

Broader Impacts. In recent years, the editing and manipulation of digital media have become increasingly convenient and widespread. Advances in image editing software, along with deep generative models such as Generative Adversarial Networks and diffusion models, make image manipulations, often imperceptible to the human eye, easier. These technologies are even widely used by potential malicious users. The widespread use of smartphones and social networks has also accelerated the dissemination of these manipulated media. Therefore, when these edited images are used to support false information activities or confuse news content to mislead the public, they can cause social issues and lead to a crisis of trust. Hence, IMDPrompter, as an effective image manipulation detection method, can significantly mitigate the problems caused by intentional image manipulation.

6.2 DATASET DESCRIPTION

In order to directly compare with state-of-the-art technologies, we trained on CASIAv2 Dong et al. (2013) and conducted extensive testing on COVER Wen et al. (2016), Columbia Hsu & Chang (2006), NIST16 Hsu & Chang (2006), CASIAv1 Dong et al. (2013), and the recent IMD Novozamsky et al. (2020).

Table 7: Details of the training set and five test sets used in our experiments. The symbol “-” indicates unavailable information. Copy-move, splicing, and inpainting operations are denoted as cpmv, spli, and inpa, respectively. Our model was trained on the CASIAv2 dataset and evaluated across all test sets.

Dataset	Negative	Positive	cpmv	spli	inpa
Training					
CASIAv2 Dong et al. (2013)	7491	5063	3235	1828	0
Testing					
COVER Wen et al. (2016)	100	100	100	0	0
Columbia Hsu & Chang (2006)	183	180	0	180	0
NIST16 Dong et al. (2013)	0	564	68	288	208
CASIAv1+ Dong et al. (2013)	800	920	459	461	0
IMD Novozamsky et al. (2020)	414	2010	-	-	-

6.3 BASELINE METHODS

As shown in Table 8, we have organized the technical routes of the baseline methods. To ensure fair and reproducible comparisons, we selected state-of-the-art models that meet any of the following criteria: 1) pretrained models released by the paper authors, 2) publicly available source code, and 3) adherence to a common evaluation protocol, where CASIAv2 is used for training and other public datasets for testing. Based on these criteria, we compiled a list of nine published baselines, as follows:

- H-LSTM Bappy et al. (2019): Pretrained on a custom dataset of 65k processed images and fine-tuned on NIST16 and IEEE Forensics Challenge data.
- ManTra-Net Wu et al. (2019): Trained on millions of processed images in a private collection.

Table 8: Comparison of Technical Routes of Baseline Methods

Method	View			Semantic Segmentation Backbone
	RGB	Noise	Fusion	
MFCNSalloum et al. (2018)	+	-	-	FCN
RGB-NZhou et al. (2018b)	+	SRM	Late Fusion(Bilinear Pooling)	Faster R-CNN
H-LSTM Bappy et al. (2019)	+	-	-	Patch-LSTM
ManTra-NetWu et al. (2019)	+	SRM+Bayar	Early Fusion(Feature Concatenation)	Wider VGG
HP-FCN Li & Huang (2019)	-	High-pass filters	-	FCN
GSR-NetZhou et al. (2018a)	+	-	-	DeepLabv2
CR-CNN Yang et al. (2020)	-	Bayar	-	Mask R-CNN
SPAN Hu et al. (2020)	+	SRM+Bayar	Early Fusion(Feature Concatenation)	Wider VGG
MM-Net Yang et al. (2021)	+	Bayar	Middle Fusion(Attention Guidance)	Mask R-CNN
JPEG-ComNet Rao & Ni (2021)	+	SRM	Early Fusion(Feature Concatenation)	Siamese FCN
CAT-Net Kwon et al. (2021)	+	DCT	Middle Fusion(Feature Concatenation)	HRNet
MVSS-Net Chen et al. (2021)	+	Bayar	Late Fusion(Dual Attention)	FCN
TruFor Guillaro et al. (2023)	+	Noiseprint	Late Fusion(Feature Concatenation)	Segformer
IMDPrompter	+	SRM+Bayar+Noiseprint	Late Fusion(Optimal Prompt Selection +Cross-view Prompt Consistency)	FCN+SAM

- HP-FCN Li & Huang (2019): Trained on a private set of repaired images.
- CR-CNN Yang et al. (2020): Trained on CASIAv2.
- SPAN Hu et al. (2020): Trained using the same data as ManTra-Net and fine-tuned on CASIAv2.
- CAT-Net Kwon et al. (2021): Trained on a joint dataset including CASIAv2, IMD, Fantastic Reality Kniaz et al. (2019), and self-spliced COCO.

For models with publicly available code, we trained them using the code provided by the authors, such as GSR-Net Zhou et al. (2018a). When citing their results, we adopt the original data where appropriate and only use our retrained models when necessary. For models that follow the same evaluation protocol, such as MFCN Salloum et al. (2018) and RGB-N Zhou et al. (2018b), we directly cite results from the same team Yang et al. (2020). For fair comparison, we retrained FCN Long et al. (2015), MVSS-Net Dong et al. (2022), and TruFor Guillaro et al. (2023) from scratch on CASIAv2. As previous studies rarely report their image-level performance, these models typically lack an image classification head in their implementations. To obtain a baseline for image-level predictions without modifying their models or code, we adopted the GMP strategy used in MVSS-Net.

6.4 SUPPLEMENTARY EXPERIMENTS

Experimental Setups. To improve reproducibility, we present the used parameters details in Table 9.

Overall Performance in Detection and Localization. Table 10 and Figure 6 shows the overall performance of pixel-level and image-level manipulation detection. We use the harmonic mean of image-level detection F1 and pixel-level localization F1, denoted as C-F1, as our overall performance metric. As shown in Table 3, IMDPrompter achieves the best performance in all settings, with a performance improvement of 45.3% over the next best method. Notably, in the experiments on the COVER dataset, we achieved a performance gain of 110.7%.

Ablation study of the segmenters for the four prompt views: We selected several segmenters, including FCN, PSPNet, SETR, and Segformer, for ablation experiments. As shown in the table below, the lightweight FCN based on MobileNet is sufficient to effectively guide SAM’s automated prompt learning. The introduction of more powerful segmenters like PSPNet, SETR, and Segformer did not result in a significant improvement in detection performance but instead introduced greater computational overhead. Therefore, we chose the lightweight FCN as our segmenter.

Computational Complexity Analysis: As shown in Table 15, I-AUC represents Image-level AUC, I-F1 represents Image-level F1, P-F1 represents Pixel-level F1, and C-F1 represents the harmonic mean of I-F1 and P-F1. It is worth noting that the IMDPrompter mentioned in the main text is based on SAM-H, which has a high computational complexity. Therefore, we implemented a lightweight version, IMDPrompter*, based on Mobile SAM. As can be seen from Table 15, IMDPrompter achieved the best performance on almost all metrics, and IMDPrompter* achieved performance second only to IMDPrompter in nearly all metrics.

Table 9: Parameter Settings Details

Parameter	Value
Warm-up Learning Rate Scheduler	
Type	LinearLR
Start Factor	1.00E-04
By Epoch	TRUE
Begin	0
End	1
Convert to Iter Based	TRUE
Main Learning Rate Scheduler	
Type	CosineAnnealingLR
T_max	max_epochs
By Epoch	TRUE
Begin	1
End	max_epochs
Data Preprocessor	
Mean	[123.675, 116.28, 103.53]
Standard Deviation	[58.395, 57.12, 57.375]
BGR to RGB	TRUE
Padding Value	0
Segmentation Padding Value	255
Size	-10,241,024
Trainer	
Number of Things Classes	2
Train Batch Size per GPU	1
Train Number of Workers	4
Test Batch Size per GPU	1
Test Number of Workers	4
Epochs	100

Table 10: Overall Detection and Localization Performance (Com-F1 Score). The best results for each test set are highlighted in bold and second-best values are underlined.

Method	CASIA	COVER	Columbia	IMD	MEAN
H-LSTM Bappy et al. (2019)	0.0	0.0	3.8	0.0	0.94
ManTra-Net Wu et al. (2019)	0.0	0.0	0.0	0.0	0.00
CR-CNN Yang et al. (2020)	30.3	18.1	41.3	23.7	28.35
GSR-Net Zhou et al. (2018a)	0.0	0.0	4.2	0.0	1.06
SPAN Hu et al. (2020)	0.0	0.0	0.0	0.0	0.00
CAT-Net Kwon et al. (2021)	20.0	19.7	69.1	9.5	29.59
MVSS-Net Chen et al. (2021)	<u>56.6</u>	<u>31.7</u>	<u>71.1</u>	<u>30.0</u>	<u>47.36</u>
FCN Long et al. (2015)	53.6	18.9	30.5	23.3	31.57
IMDPrompter	+23.2	+47.9	+59.8	+18.0	+37.25

Comparison with SAM-based Methods: As shown in Table 15, We supplement the performance of four SAM-based image segmentation methods: MedSAM, MedSAM-Adapter, AutoSAM, and SAMed. As we can see, these four SAM-based methods exhibit limited performance in the image manipulation detection task due to their reliance solely on semantically relevant information. In particular, there is a significant performance gap between them and IMDPrompter, especially on the out-of-domain test sets CVOER, Columbia, and IMD.

Proportion of Four Views Selected as Optimal Prompts. As shown in Table 17, we summarize the proportion of each prompt view being selected as the optimal prompt during training. We observe that the RGB view is selected as the optimal prompt in only 13.9% of cases, indicating that

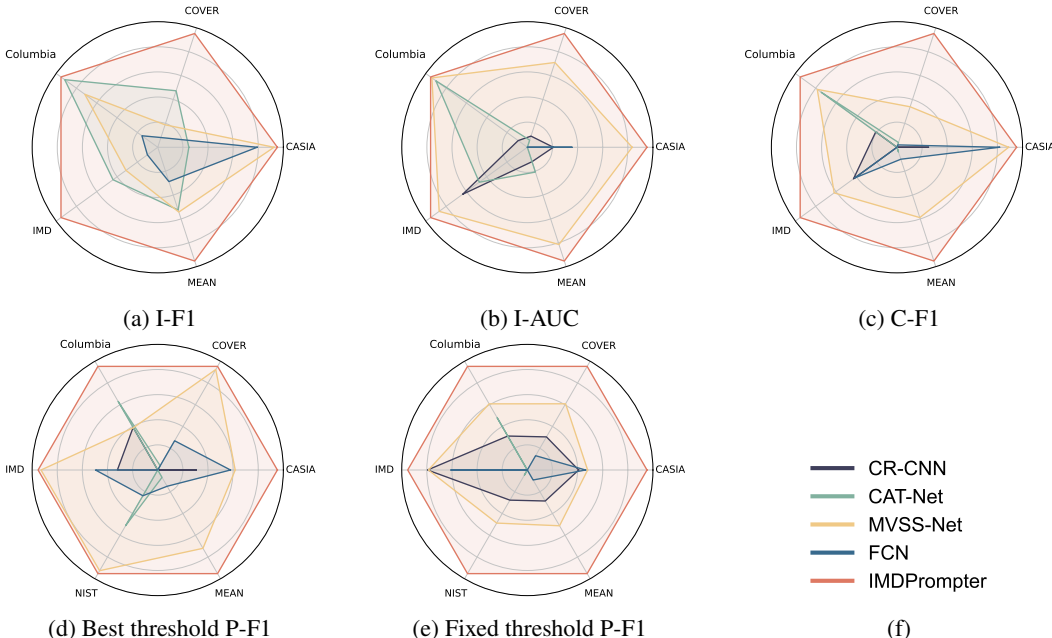


Figure 6: Visualization of Metric Data Comparison between IMDPrompter and State-of-the-Art (SOTA) Methods

Table 11: Impact of JPEG Compression and Gaussian Blur on Pixel-level F1

Method	JPEG Compression						Gaussian Blurs					
	100	90	80	70	60	50	0	5	11	17	23	29
H-LSTM Bappy et al. (2019)	15.4	15.0	14.8	14.7	14.0	13.9	15.4	13.4	12.1	10.8	10.6	10.3
ManTra-Net Wu et al. (2019)	15.5	11.9	8.2	8.0	8.7	8.6	15.5	12.0	11.3	12.0	11.6	11.2
CR-CNN Yang et al. (2020)	40.4	33.6	22.4	17.1	11.7	9.2	40.4	23.3	22.1	21.1	20.7	19.9
GSR-Net Zhou et al. (2018a)	37.4	35.9	32.5	32.4	30.8	27.0	37.4	30.5	26.5	23.5	20.8	19.0
SPAN Hu et al. (2020)	18.2	17.1	17.1	16.6	15.7	14.9	18.2	10.7	10.6	10.0	9.6	9.6
CAT-Net Kwon et al. (2021)	13.5	2.2	2.0	1.3	0.9	0.9	13.5	9.4	9.3	6.9	6.1	6.0
MVSS-Net Chen et al. (2021)	45.1	43.2	42.5	41.2	40.2	39.5	45.1	37.4	36.0	33.0	21.1	17.3
IMDPrompter	76.3	73.6	72.0	71.6	70.7	70.5	76.3	71.8	71.1	68.8	56.6	51.6

semantically relevant features alone are insufficient to guide SAM’s prompt learning. On the other hand, the Noiseprint view is chosen as the optimal prompt in 46.3% of cases, demonstrating that the semantically irrelevant information provided by Noiseprint is the most crucial.

Hyperparametric Analysis As shown in Figure 7, we conducted hyperparameter analysis on $\lambda_1, \lambda_2,$ and $\lambda_3,$ ultimately selecting the optimal parameter configuration: $\lambda_1 = 1.0, \lambda_2 = 0.1, \lambda_3 = 1.0.$

Performance of Generative Image Manipulation Detection: Following the work of Trufor, we supplement the performance of IMDPrompter on CocoGlide (image tampering based on diffusion models). As shown in the table below, our IMDPrompter also achieves objective results for AIGC-edited images.

Impact of Quality Degradation. As shown in Table 11,12,13, following Dong et al. (2022), we evaluated the robustness of the models under two common image processing operations encountered during the dissemination of images on the internet, namely JPEG compression and Gaussian blur. Comparing these two operations, Gaussian blur has a more significant impact on detection performance, especially when using larger 17x17 scale convolution kernels. Compared to previous methods, our IMDPrompter exhibits better robustness.

More Visualization. As shown in Figure 10, we have included additional visualizations.

Table 12: Impact of JPEG Compression and Gaussian Blur on Image-level F1

Method	JPEG Compression						Gaussian Blur					
	100	90	80	70	60	50	0	5	11	17	23	29
H-LSTM Bappy et al. (2019)	0.0	0.0	0.0	0.0	0.0	0.0	0.0	0.0	0.0	0.0	0.0	0.0
ManTra-Net Wu et al. (2019)	0.0	0.0	0.0	0.0	0.0	0.0	0.0	0.0	0.0	0.0	0.0	0.0
CR-CNN Yang et al. (2020)	24.3	25.8	24.0	22.4	20.0	18.4	24.3	14.3	13.9	13.7	12.4	11.4
GSR-Net Zhou et al. (2018a)	0.0	0.0	0.0	0.0	0.0	0.0	0.0	0.0	0.0	0.0	0.0	0.0
SPAN Hu et al. (2020)	0.0	0.0	0.0	0.0	0.0	0.0	0.0	0.0	0.0	0.0	0.0	0.0
CAT-Net Kwon et al. (2021)	38.0	17.9	17.2	15.0	12.4	11.0	38.0	11.9	11.0	10.5	10.3	10.7
MVSS-Net Chen et al. (2021)	75.9	76.2	75.7	75.3	74.8	73.0	75.9	73.8	72.8	70.7	65.8	63.4
IMDPrompter	77.3	77.8	77.2	76.8	76.1	74.6	77.3	75.9	74.6	73.1	69.3	66.6

Table 13: Impact of JPEG Compression and Gaussian Blur on Com-F1

Method	JPEG Compression						Gaussian Blur					
	100	90	80	70	60	50	0	5	11	17	23	29
H-LSTM Bappy et al. (2019)	0.0	0.0	0.0	0.0	0.0	0.0	0.0	0.0	0.0	0.0	0.0	0.0
ManTra-Net Wu et al. (2019)	0.0	0.0	0.0	0.0	0.0	0.0	0.0	0.0	0.0	0.0	0.0	0.0
CR-CNN Yang et al. (2020)	30.3	29.2	23.2	19.4	14.8	12.3	30.3	17.7	17.0	16.6	15.5	14.5
GSR-Net Zhou et al. (2018a)	0.0	0.0	0.0	0.0	0.0	0.0	0.0	0.0	0.0	0.0	0.0	0.0
SPAN Hu et al. (2020)	0.0	0.0	0.0	0.0	0.0	0.0	0.0	0.0	0.0	0.0	0.0	0.0
CAT-Net Kwon et al. (2021)	19.9	3.9	3.6	2.3	1.7	1.7	19.9	10.5	10.1	8.3	7.7	7.7
MVSS-Net Chen et al. (2021)	56.6	55.1	54.4	53.2	52.3	51.2	56.6	49.7	48.2	45.0	32.0	27.2
IMDPrompter	76.8	75.6	74.5	74.1	73.3	72.5	76.8	73.8	72.8	70.9	62.3	58.1

Table 14: Ablation Study of the Segmenter

	Params/M	GFLOPs	CASIA			COVER			Columbia			IMD						
			I-AUC	I-F1	P-F1	C-F1	I-AUC	I-F1	P-F1	C-F1	I-AUC	I-F1	P-F1	C-F1				
PSPNetZhao et al. (2017)	365.3	1610.3	0.979	77.4	76.5	76.9	0.794	70.3	63.7	66.8	0.984	93.7	87.8	90.7	0.673	64.1	30.6	41.4
SPANHu et al. (2020)	15.4	30.9	0.500	0.0	18.4	0.0	0.500	0.0	17.2	0.0	0.500	0.0	48.7	0.0	0.500	0.0	17.0	0.0
SETRZheng et al. (2021)	1591.6	2131.6	0.985	78.1	77.1	77.6	0.801	70.9	64.3	67.4	0.988	94.1	88.2	91.1	0.679	64.5	31.1	42.0
SegformerXie et al. (2021)	536.3	1769.3	0.988	78.9	77.8	78.3	0.811	71.2	65.1	68.0	0.991	94.9	88.7	91.7	0.684	65.1	32.1	43.0
FCNLong et al. (2015)	347.6	1533.2	0.978	77.4	76.4	76.9	0.795	70.2	63.7	66.8	0.984	93.6	87.6	90.5	0.670	63.8	30.6	41.4

Table 15: Computational Complexity Overhead

	Params/M	GFLOPs	CASIA			COVER			Columbia			IMD						
			I-AUC	I-F1	P-F1	C-F1	I-AUC	I-F1	P-F1	C-F1	I-AUC	I-F1	P-F1	C-F1				
ManTra-NetWu et al. (2019)	4.0	1009.7	0.500	0.0	15.5	0.0	0.500	0.0	28.6	0.0	0.701	0.0	36.4	0.0	0.500	0.0	18.7	0.0
SPANHu et al. (2020)	15.4	30.9	0.500	0.0	18.4	0.0	0.500	0.0	17.2	0.0	0.500	0.0	48.7	0.0	0.500	0.0	17.0	0.0
MVSS-NetChen et al. (2021)	146.9	160.0	0.937	75.8	75.2	76.6	0.731	24.4	45.3	31.7	0.980	80.2	63.8	71.1	0.656	35.5	26.0	30.0
TruorGuillaro et al. (2023)	67.8	90.1	0.916	-	44.1	-	0.770	-	19.9	-	0.996	-	22.3	-	-	-	21.0	-
IMDPrompter	347.6	1533.2	0.978	77.3	76.3	76.8	0.796	70.3	63.6	66.8	0.983	93.6	87.3	90.3	0.671	63.7	30.6	41.3
IMDPrompter*	85.8	151.3	0.951	76.1	70.3	73.1	0.779	64.5	57.7	60.9	0.980	88.3	81.6	84.8	0.667	56.9	26.9	36.5

Table 16: Comparison with SAM-based methods.

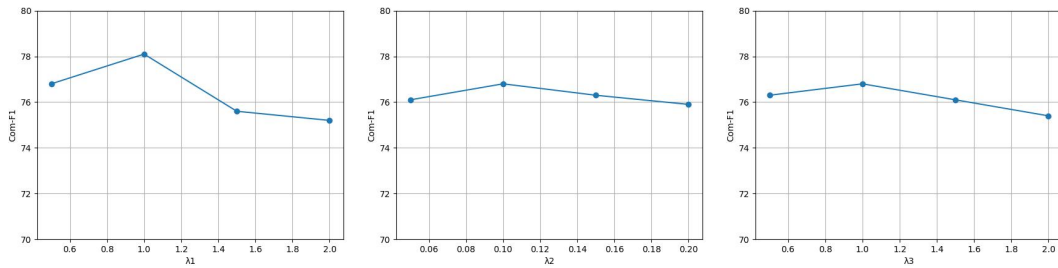
	CASIA			COVER			Columbia			IMD						
	I-AUC	I-F1	P-F1	C-F1	I-AUC	I-F1	P-F1	C-F1	I-AUC	I-F1	P-F1	C-F1				
MedSAMMa et al. (2024)	0.861	70.3	56.4	62.6	0.563	26.3	22.1	24.0	0.791	50.1	24.6	33.0	0.513	26.1	22.4	24.1
MedSAM-AdapterWu et al. (2023)	0.877	71.0	57.3	63.4	0.543	21.6	20.3	20.9	0.742	46.6	22.1	30.0	0.494	25.1	21.6	23.2
AutoSAMShaharabany et al. (2023)	0.843	69.1	55.1	61.3	0.513	18.9	18.6	18.7	0.772	49.1	28.4	36.0	0.523	27.9	22.9	25.2
SAMedZhang & Liu (2023)	0.843	69.9	52.3	59.8	0.571	27.6	24.6	26.0	0.801	53.1	31.7	39.7	0.502	27.6	23.1	25.2
IMDPrompter	0.978	77.3	76.3	76.8	0.796	70.3	63.6	66.8	0.983	93.6	87.3	90.3	0.671	63.7	30.6	41.3
IMDPrompter*	0.951	76.1	70.3	73.1	0.779	64.5	57.7	60.9	0.980	88.3	81.6	84.8	0.667	56.9	26.9	36.5

Table 17: The proportion of each view selected as the optimal view

Prompt View	RGB	SRM	Bayer	Noiseprint
Percent	13.9%	18.4%	21.4%	46.3%

Table 18: Performance of Generative Image Manipulation Detection

Method	CocoGlide			
	P-F1(best)	P-F1(fixed)	I-AUC	I-Acc
ManTraNet Wu et al. (2019)	0.673	0.516	0.778	0.500
SPAN Hu et al. (2020)	0.35	0.298	0.475	0.491
MVSS-Net Chen et al. (2021)	0.642	0.486	0.654	0.536
Trufor Guillaro et al. (2023)	0.72	0.523	0.752	0.639
IMDPrompter	0.746	0.539	0.781	0.652

Figure 7: Hyperparametric analysis of λ_1 , λ_2 , and λ_3

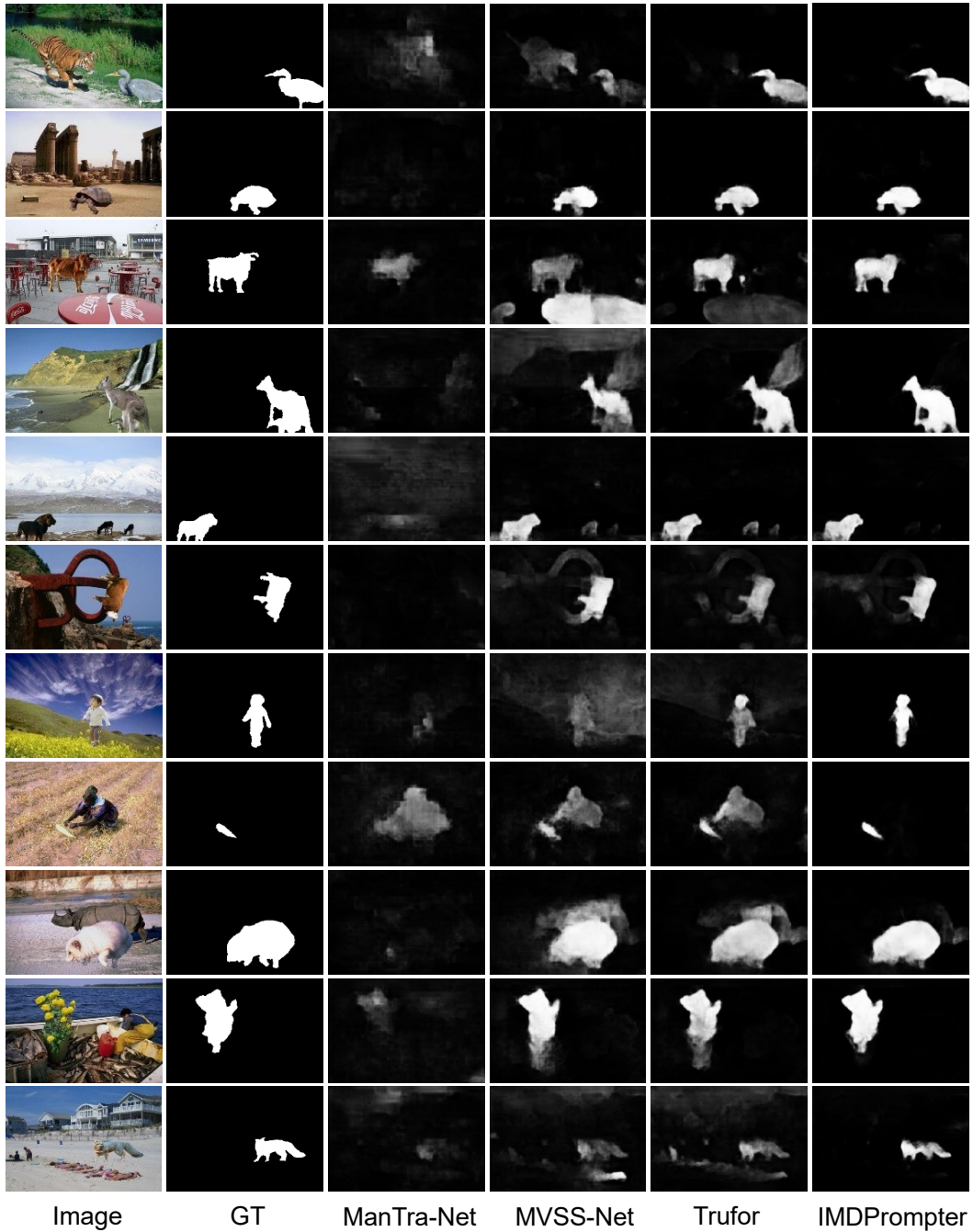


Figure 8: Some qualitative results, compared with the state-of-the-art

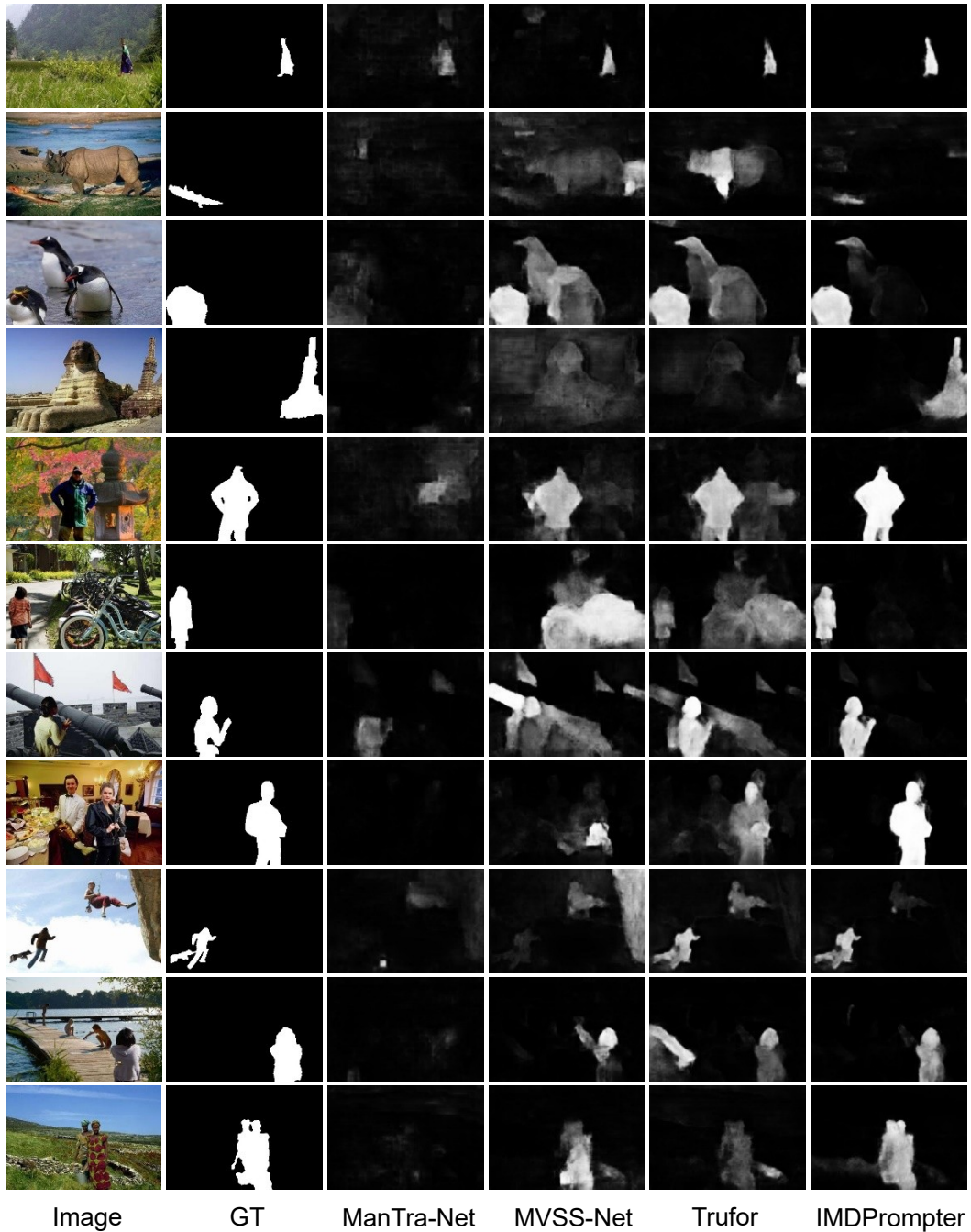


Figure 9: Some qualitative results, compared with the state-of-the-art

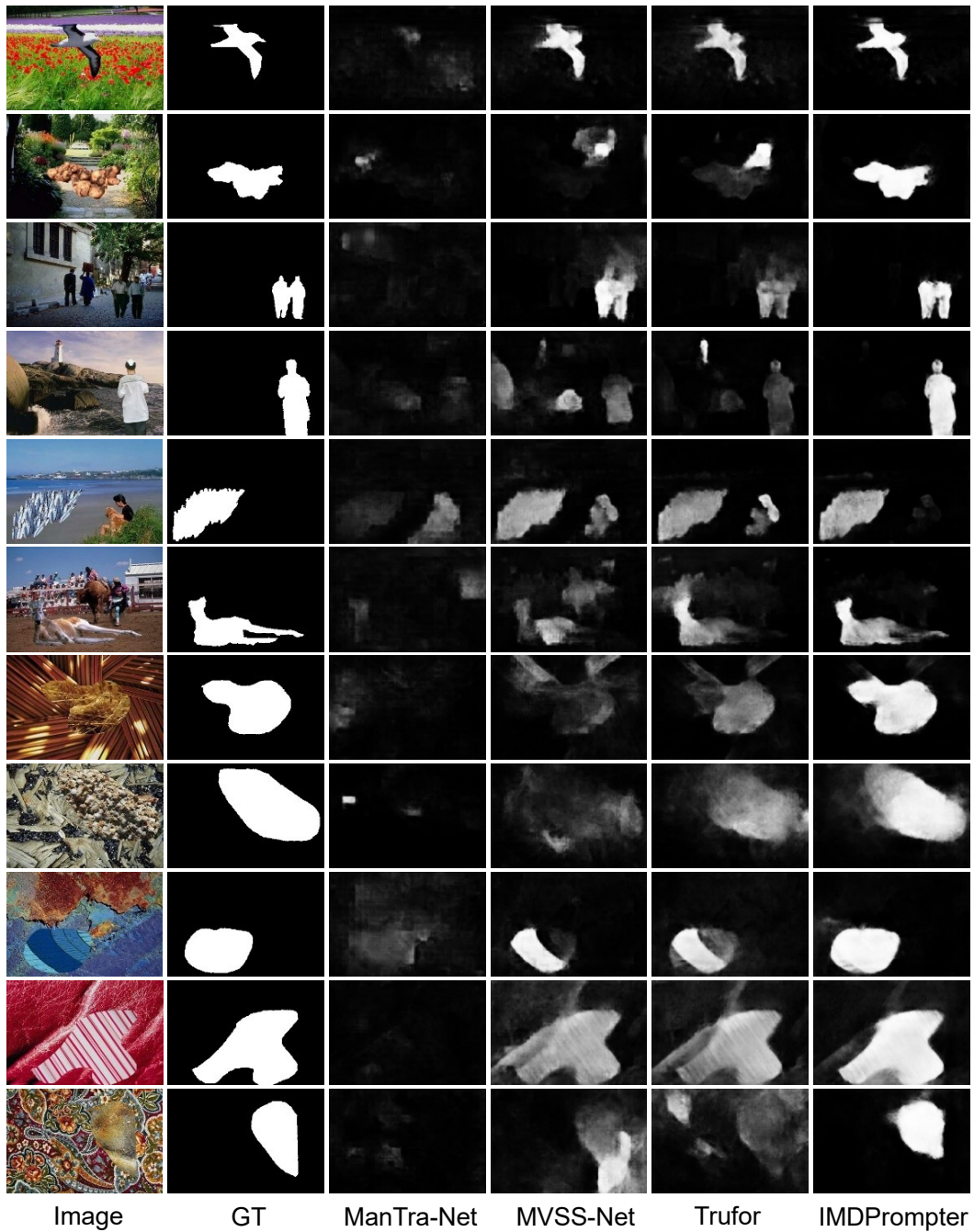


Figure 10: Some qualitative results, compared with the state-of-the-art